General Disclaimer

One or more of the Following Statements may affect this Document

- This document has been reproduced from the best copy furnished by the organizational source. It is being released in the interest of making available as much information as possible.

- This document may contain data, which exceeds the sheet parameters. It was furnished in this condition by the organizational source and is the best copy available.

- This document may contain tone-on-tone or color graphs, charts and/or pictures, which have been reproduced in black and white.

- This document is paginated as submitted by the original source.

- Portions of this document are not fully legible due to the historical nature of some of the material. However, it is the best reproduction available from the original submission.

Produced by the NASA Center for Aerospace Information (CASI)

NASA TECHNICAL MEMORANDUM

NASA TM-73887

NASA TM-73887

(NASA-TM-73887) THE ROLE OF DROP VELOCITY IN STATISTICAL SPRAY DESCRIPTION (NASA) 14 p HC A02/MF A01 CSCL 20D

N78-20458

Unclas
G3/34 09481

THE ROLE OF DROP VELOCITY IN STATISTICAL SPRAY DESCRIPTION

by J. F. Groeneweg
Lewis Research Center
Cleveland, Ohio 44135

and

M. M. El-Wakil, P. S. Myers, and O. A. Uyehara
University of Wisconsin
Madison, Wisconsin

TECHNICAL PAPER to be presented at the
First International Conference on Liquid
Atomization and Spray Systems
Tokyo, Japan, August 29-31, 1978

THE ROLE OF DROP VELOCITY IN STATISTICAL SPRAY DESCRIPTION

J. F. Groeneweg,[1] M. M. El-Wakil,[2] P. S. Myers,[2] and O. A. Uyehara[2]

E-9502

ABSTRACT

The justification for describing a spray by treating drop velocity as a random variable on an equal statistical basis with drop size was studied experimentally. A double-exposure technique using fluorescent drop photography was used to make size and velocity measurements at selected locations in a steady ethanol spray formed by a swirl atomizer. The size-velocity data were categorized to construct bivariate spray density functions to describe the spray immediately after formation and during downstream propagation. It was found that a statistical treatment of drop velocity was supported by the data. Spray density function shapes and modal characteristics depended strongly on position and the amount of droplet-gas interaction that had occurred. Bimodal density functions were formed by environmental interaction during downstream propagation. Large differences were also found between spatial mass density and mass flux size distributions at the same location.

NOMENCLATURE

- D = drop diameter, μm
- f = spray density function, no. drops per unit size, velocity, position, drop temperature
- f_E = measured spray density function, no. drops/(μm·cm/s·cm^3), Eqs. (11) and (12)
- $\underline{f}_F$ = flux drop size distribution, no. of drops/(μm·cm^2·s)
- f_S = spatial drop-size distribution, no. of drops/(μm·cm^3)
- f_V = velocity distribution, no. of drops/(cm/s)
- f_z = one-dimensional spray density, no. of drops/(μm·cm·cm/s), Eqs. (12) and (18)
- g = function of drop variables, Eq. (2)
- M = drop mass, $\rho_L \pi D^3/6$, g/cc
- m = constant in Eq. (13)
- N = total no. of drops
- n_{ijk} = no. of drops in i^{th} size, j^{th} axial velocity, and k^{th} radial velocity categories
- r = radial coordinate, cm
- T_L = temperature of drop, K
- t = time, s
- u = gas velocity in spray, cm/s
- V_s = sampling volume, cm^3
- v_E = liquid exit velocity, cm/s
- v_{zs} = axial velocity of liquid sheet, cm/s
- $\underline{v}$ = drop velocity vector, cm/s, components in cylindrical coordinates, v_r, v_θ, v_z
- w = weighting function, Eq. (2)
- $\underline{x}$ = position vector, cm
- z = axial coordinate, mm
- ϵ = no. of photographic samples at given spray condition
- Γ_i = general drop variable
- $\Delta\Gamma$ = increment in Γ_i
- ρ_L = drop density, g/cm^3
- ρ_s = spray density, g/cm^3
- $\underline{\ }$ = underline -- vector
- $\bar{\ }$ = ensemble average
- $\langle\ \rangle_M$ = ensemble average weighted by M
- $\hat{\ }$ = average in category
- $'$ = particular location

INTRODUCTION

In the hundreds of spray studies which have been conducted over the past century droplet size has received the most emphasis as the key variable in spray description. It has long been recognized that the atomization process is random as far as the sizes of the droplets formed and a statistical treatment in terms of size distributions and associated means is used. The situation with respect to other droplet independent variables such as velocity is much less clear.

A general statistical mechanical theory of sprays has been formulated [1] which includes size, velocity, and position as independent variables, but applications of the theory have been primarily limited to considerations of the statistical properties of drop size. While some measurements of drop velocity have been made [2,3,4,5], velocity has not been purposely treated as a random variable on an equal statistical basis with drop size. Data have been interpreted on the supposition that drops of a given size all move with the same average velocity at a given location in the spray.

However, physical examination of the spray situation leads to the conclusions that (a) spray formation is a random process which is distributed in space and (b) the histories of individual droplets are unique functions of the initial conditions and later environment. These conditions imply that, at downstream locations where a collection of approximately spherical drops first exists, other droplet properties besides

[1] Lewis Research Center, National Aeronautics and Space Administration, Cleveland, Ohio

[2] University of Wisconsin, Madison, Wisconsin

ORIGINAL PAGE IS
OF POOR QUALITY

size should be treated as being statistically distributed.

The investigation described in this paper explor[es] the justification for and consequences of treating drop velocity as a random variable on an equal statistical basis with drop size. The approach was basically an experimental one in which detailed measurements of drop size and velocity were made at selected locations in a spray. The measurements were analyzed in terms of a spray density function which is based on a statistical mechanics approach to spray description. Specific goals of the study were to determine if data support such a statistical treatment of drop velocity and to examine the implications of such a treatment for interpreting size data and analyzing spray behavior. Because of the difficulties in measuring sizes and velocities and the large number of measurements required, the scope of the investigation was limited to a detailed characterization of one particular spray situation.

SUMMARY OF STATISTICAL SPRAY DESCRIPTION

For purposes of this discussion, spray studies are divided into the two general areas of formation and propagation. Formation concerns the process by which liquid in a reservoir is atomized. The description of the resultant spray depends upon initial conditions of fluid properties, atomizer geometry, energy addition and properties of the medium in which the spray is formed. Propagation involves the description of changes in spray properties due to transfer processes which occur in the two-phase flow downstream. The conceptual boundary separating these two regimes may be called the surface of formation. Describing the spray at this interface is the endpoint of formation studies and the initial condition for propagation studies. The method of describing the spray in terms of a spray density function at the surface of formation and some aspects of its propagation are the main emphases in this paper.

Spray Density Function

Consider a function $f(\Gamma_i,t)$ as a representation of the spray at the surface of formation. The variables Γ_i are randomly distributed and are chosen as those properties necessary to describe the droplet state at formation and during subsequent propagation, that is, drop mass, momentum and energy at any location. Therefore, reasonable choices for Γ_i are size D, position $\underline{x}$, velocity $\underline{v}$, and temperature T_L. The inclusion of T_L is a generalization of the treatment in reference 1 and is discussed in detail in reference 6. The function f represents the probable number of drops in the range $d\Gamma_i$ about Γ_i at a time t. In this unnormalized form:

$$N = \int_{\text{all } \Gamma_i} f(\Gamma_i,t)d\Gamma_i \qquad (1)$$

where N is the total number of drops represented by f at a time t.

Ensemble averages or moments of a function $g(\Gamma_i,t)$ when weighted by another function $W(\Gamma_i)$ are given by:

$$\langle g(\Gamma_i,t)\rangle_W = \frac{\int W(\Gamma_i)g(\Gamma_i,t)f(\Gamma_i,t)d\Gamma_i}{\int W(\Gamma_i)f(\Gamma_i,t)d\Gamma_i} \qquad (2)$$

For example, the mass average velocity is given by:

$$\langle \underline{v}\rangle_M = \frac{\iiint M\underline{v}f\, dD\, d\underline{v}\, dT_L}{\iiint Mf\, dD\, d\underline{v}\, dT_L} \qquad (3)$$

where $\langle \underline{v}\rangle_M$ remains a function of position $\underline{x} = \underline{x}'$ and M is the droplet mass, $\rho_L\pi D^3/6$. The denominator of Eq. (3) is the spray density ρ_s:

$$\rho_s = \iiint Mf\, dD\, d\underline{v}\, dT_L \qquad (4)$$

Various marginal density functions may be defined in which all independent variables except one are integrated out mathematically or disregarded experimentally. The marginal density on Γ_i is:

$$f(\Gamma_i) = \int f(\Gamma_i,\Gamma_j,t)d\Gamma_j \qquad i \neq j \qquad (5)$$

where, as usual, the integrals are over the whole range of Γ_j. A particular marginal density is the usual spatial drop size distribution:

$$f_s(D,x',t) = \iint f(D,\underline{v},\underline{x}',T_L,t)d\underline{v}\, dT_L \qquad (6)$$

Similarly, the "velocity distribution" is:

$$f_v(\underline{v},x',t) = \iint f(D,\underline{v},\underline{x}',T_L,t)dD\, dT_L \qquad (7)$$

Another marginal size distribution of interest is the temporal or flux size distribution given by:

$$\underline{f}_F(D,\underline{x}',t) = \iint \underline{v}f(D,\underline{x}',\underline{v},T_L,t)d\underline{v}\, dT_L \qquad (8)$$

The physical significance of f_s and $\underline{f}_F$ are as follows. The spatial distribution is the number of drops per unit spatial volume per unit size at a time t and is measured by instantaneous photographs of drops in a known spatial volume. The flux distribution is the number of drops per unit area per unit size and time collected as they cross a known surface area averaged over time. Equation (8) defines the flux distribution in a way which is equivalent to the one obtained by collection if the spray is a stationary random process with time averages equal to ensemble averages.

The average (expected value) of any function $g(\Gamma_i)$ for a given value of the spray variable Γ_j is defined for $i \neq j$ as:

$$\langle f(\Gamma_i|\Gamma_j)\rangle = \frac{\int g(\Gamma_i)f(\Gamma_i,\Gamma_j,t)d\Gamma_i}{\int f(\Gamma_i,\Gamma_j,t)d\Gamma_i} \qquad (9)$$

A particular case of interest is the expected value of velocity at a given size as a function of D and $\underline{x}'$ given by:

$$\langle \underline{v}|D\rangle = \frac{\iint \underline{v}f(D,\underline{v},x',T_L,t)d\underline{v}\, dT_L}{\iint f(D,\underline{v},\underline{x}',T_L,t)d\underline{v}\, dT_L} = \frac{\underline{f}_F}{f_s} \qquad (10)$$

It has been estimated experimentally by averaging measured velocities of particular sized drops [3,4,5] but was not interpreted as being derived from a density function f which contained $\underline{v}$ as a randomly distributed variable. Equation (10) also shows that $\langle \underline{v}|D\rangle$ is given by the ratio of flux to spatial size distributions.

This brief summary of density functions, derived forms and means is sufficient for the interpretation

ORIGINAL PAGE IS
OF POOR QUALITY

of the data to be presented. For a more detailed discussion of equations of change for f and associated means, see Refs. [1] and [6].

MEASUREMENT OF THE SPRAY DENSITY FUNCTION

The particular form of the density function measured was restricted to the variables D, $\underline{v}$, and $\underline{x}$. Droplet temperature was not measured which was equivalent to integrating over T_L. Injection parameters were held constant so that a steady-state spray condition was assumed eliminating consideration of time, t. In terms of the general f, the measured density f_E is:

$$f_E(D,\underline{v},\underline{x}') = \int f(D,\underline{v},\underline{x}',T_L,t)dT_L \qquad (11)$$

where $\underline{x}'$ indicates that the functions are evaluated at a particular spray position, $\underline{x} = \underline{x}'$. Symmetry was assumed about the spray axis, and only two components of position and velocity were considered in cylindrical coordinates: r, z, v_r, and v_z. Any v_θ was normal to the sampling plane and could not be measured.

Fluorescent Spray Photography

A double-exposure fluorescent technique was used to measure sizes and velocities. This method left the spray undisturbed and provided direct local values of the droplet variables. The fluorescent technique of photographing droplets was originally developed [7,8] as a single exposure method of measuring the sizes of drops in a small spatial volume at any instant to give the spatial drop size distribution, f_s. In the present study a precisely controlled double-exposure capability was added to provide a measure of droplet velocity as well as size so that f_E could be estimated.

The key feature of the technique is the addition of a fluorescent dye to the liquid being sprayed. A shaped light beam selectively lights a region of the spray and defines the sampling volume on which the camera is focused. Only drops within the camera's depth of field are lighted and caused to fluoresce. Multiple exposures may be recorded without loss of contrast since each fluorescing droplet is a primary source recording its image with an unlighted background.

A pictorial view of the experimental arrangement which was used is shown in Fig. 1. The axes of the spray, camera and lighting system are mutually perpendicular. Liquid containing the fluorescent dye was injected vertically from a swirl atomizer, passed through the region where sampling occurred, and was collected and removed from the room by an exhaust system. Identical lighting systems consisting of constricted spark gaps and quartz condensing lenses having specially shaped aperture stops were located on either side of the camera axis. When either gap was fired the condenser lenses focused and shaped the beam to light the same volume in the spray. The firing sequence of the two sources was monitored by a phototube and controlled to produce two flashes separated by a known time interval. Each drop within the sampling volume viewed by the camera successively fluoresced and was recorded twice on the film. The position of the camera and lighting system was fixed to maintain alignment, and the nozzle was positioned so that the spray could be sampled at various axial and radial locations.

Table I summarizes the specifications and operating conditions for the various elements of the sampling system. Details of the development of the lighting and camera systems and the fluorescent dye characteristics are available elsewhere [7,8]. Successful application of the fluorescent technique depends on having very intense light sources and carefully aligning the system elements.

Sampling Conditions and Data Reduction

An unconfined spray was formed by steady injection of ethyl alcohol through a swirl atomizer into a room at ambient temperature and pressure. The sampling location and injection pressure were varied as shown in the diagram of sampling geometry given in Fig. 2. A traverse of radial positions at locations immediately after breakup showed initial conditions just after spray formation for three injection pressures. Radial surveys at two downstream distances provided data on the changes that occurred during propagation. The magnitude of the air velocity in the spray was due to a combination of motion induced by the exhaust fan, which was less than 60 cm/sec over the range of positions measured, and the entrained air motion produced by the momentum transfer from the spray to the air.

The photographs were taken with the room darkened and several samples of collections of droplet image pairs were recorded on each film. The interval between flashes was chosen so that complete separation of the images was achieved for most of the image pairs. A diameter, a separation distance and an angle of the drop trajectory in the r-z plane were measured for each droplet pair. The measurements were made by hand on the screen of a microcard reader at additional magnifications of 16 to 18 times. From these measurements the size D and two components of velocity, v_r and v_z, were calculated for each drop. The conical liquid sheet velocity before breakup was also measured from double exposure photographs. A total of more than 30,000 pairs of drop images were measured and the data were processed on a digital computer.

ANALYSIS OF THE SIZE-VELOCITY DATA

The density function f_E is estimated by categorizing the size-velocity data and applying an approximate form to give values of f_E at the category means:

$$f_E(\hat{D}_i,\hat{v}_{zj},\hat{v}_{rk},x') = \frac{n_{ijk}}{V_s \epsilon \, \Delta D_i \, \Delta v_{zj} \, \Delta v_{rk}} \qquad (12)$$

The estimate is improved as the sample size n_{ijk} and the number of samples ϵ increase and the category sizes are decreased. Category boundaries were chosen which increased by a constant multiple so that the fractional change in D or v was a constant. For any drop variable:

$$\Gamma_i = \Gamma_1 m^{i-1} \qquad (13)$$

$$\Delta\Gamma_i = \Gamma_{i+1} - \Gamma_i \qquad (14)$$

and the category geometric mean was used:

$$\Gamma_i = (\Gamma_i \Gamma_{i+1})^{1/2} \qquad (15)$$

The values of m and Γ_1 chosen for D, v_z, and v_r were, respectively, 1.31, 1.31 and 1.75 for m and 10 μm, 38.1 cm/s and ±25.4 cm/s for the first boundary, Γ_1. Once values for f_E were obtained, any of the

marginal densities such as f_s, weighted densities such as $\underline{f}_F$ or mean quantities such as $(v_z)_M$ can be calculated by summing over the categories to approximate the integrals defined previously.

A one-dimensional density function, f_z, was obtained by integrating f_E over the cross section. In cylindrical coordinates with equal radial increments, the integral is approximated as a sum over l radial stations:

$$f_z(\hat{D}_i,\hat{v}_{zj},\hat{v}_{rk},z') = \frac{\pi(\Delta r)^2}{V_s\ \Delta D_i\ \Delta v_{zj}\ \Delta v_{rk}} \sum_l \frac{(2l-1)}{\epsilon_l} n_{ijk} \qquad (16)$$

Radial points were taken at 2 mm increments beginning at $r = 1$ mm.

Categorization of the data gave estimates of the density functions. In this paper the densities are plotted as continuous curves through data points at the category means rather than histograms. Normalized forms are used weighted by droplet mass, M. The normalized form allows comparisons of density shapes to be made at widely different conditions and the mass weighting emphasizes the larger sizes avoiding extreme skewing toward small sizes characteristic of number densities.

Marginal Density Functions

The three marginal mass weighted densities for D, v_z, and v_r are shown in Fig. 3 at the lowest injection pressure near the surface of formation. Variations with radial position are shown for each case. The curves have been drawn to emphasize their essential bimodal character with fairing through the scatter at large sizes. The spatial density in Fig. 3(a) is the usual spatial drop size distribution obtained by photographic sampling. Note the strong radial dependence with the mode at lower sizes increasing in prominence near the outside of the spray.

Figure 3(b) shows the same spray condition with axial drop velocity as the independent variable. As before, the development of an unambiguous second mode at lower velocity is shown at the outer radial locations. As will become clear, this mode corresponds to drops being decelerated to local air velocity. Finally, Fig. 3(c) shows the marginal mass density as a function of radial velocity. Two distinct modes are again present at each location. The mode at smaller velocities peaks at small negative values of v_r related to the inward flow of entrained air. Similar overall formation behavior was observed at other injection pressures.

The entire local behavior of f_E is very diverse and spatially dependent. Local values of the bivariate forms of $f_E(D,v_z,r',z')$ could be plotted with parametric cuts through the surface at constant D or constant v_z. Their overall character is similar to Fig. 3. The density properties are initially controlled primarily by the atomizer used and the spraying parameters. However, the spatial densities are radically modified by drop-gas interactions (mainly drag in this case) as propagation proceeds. Local values of air velocity determine the location of the developing low size-velocity mode which becomes more pronounced with increased travel time from the formation region. The coupling of the liquid flow with the gas produces air entrainment [9,10]. Thus, relative velocity, which is the driving force for changes in f_E, is a function of position.

Spatial and Flux Distributions

Bimodal spatial drop size distributions obtained by photographic methods have been reported by several investigators. The most similar study to the present one used a swirl atomizer injecting into stagnant air in a closed chamber [11]. Measured values of f_S were strongly dependent on location, and in many cases were decidedly bimodal. Atomization by impinging jets injecting into still air [12] and higher velocity airstreams [14,15] have also produced spatial distributions with two modes. Due to the difficulties in separating true modes from statistical fluctuations in small samples and the complexity of treating bimodal data analytically, much data has been assumed to be unimodal [8]. It is probable that reanalysis of much existing photographic data would reveal the existence of two distinct modes.

There is also a body of data obtained by collection methods [e.g. 13] or velocity weighting of spatial distributions which corresponds to the flux distribution, $\underline{f}_F$. As stated in Eq. (10) the ratio of $\underline{f}_F$ to f_S is the average drop velocity at a given size: $\langle v|D\rangle$. Figure 4 compares the two normalized distributions at a particular downstream location. From Eqs. (3), (4), and (10), the ratio of the mass-weighted, normalized forms is:

$$\frac{Mf_{Fz}}{\rho_s(v_z)_M}\left(\frac{\rho_s}{Mf_S}\right) = \frac{\langle v_z|D\rangle}{(v_z)_M} \qquad (17)$$

as is shown in Fig. 4. In this case small drops have decelerated and their spatial density has increased while the largest drops continue to move much faster. Thus, for this gas flow condition photographs show the largest population of small drops while collectors intercept a greater number of large drops. Figure 4 emphasizes the fact that the two size distributions are not equivalent and may differ substantially. Only in the special case where all drops are traveling at the same velocity are the normalized forms of $\underline{f}_F$ and f_S equal. Figure 4 also shows that the modal characteristics of $\underline{f}_F$ and f_S can be drastically different. At this downstream position the spatial size distribution indicates that drops less than about 60 μm have nearly reached the air velocity while larger drops continue to move faster and account for the mode at large sizes. But when the spatial density is weighted by the velocity regression curve to give mass flux, the dominant mode appears at large sizes with only a small inflection remaining in the small size range. The collection of regression curves (divided by $(v_z)_M$) for different radii at a downstream location appear in Fig. 5. It can be seen that these weighting curves which relate the two types of distributions reflect the stage of deceleration so that their range varies greatly from the inner to outer locations in the spray.

One-Dimensional Density Functions

A one-dimensional description of the spray at any axial location is obtained by integrating f over a cross section. In cylindrical coordinates:

$$f_z = 2\pi \int_0^\infty f_E(D,v_z,r,z) r\, dr \qquad (18)$$

The corresponding numerical approximation using experimental data is given by Eq. (16). Note that f_z is a one-dimensional "density" with units of drops per unit size, axial velocity and length in the z

direction; and fluxes obtained from f_z are simply flow rates in the axial direction.

Normalized mass densities as a function of D are shown in Fig. 6(a) for the location near the surface of formation at the three injection pressures. The small first modes show the influence of the outer regions of the spray where drop deceleration is appreciable. A shift toward smaller sizes with increasing Δp, illustrates the well known fact that the higher energy inputs produced smaller drops. Figure 6(b) shows the corresponding velocity dependence. Only small fractions of the mass have approached equilibrium with the air. The exact location and height of the low velocity mode in each case depends on how well the sampling location approximated the surface of formation and the extent of the formation region which was greatest at Δp = 1.7 atm. Nearly all of the mass is located in the second modes which broaden with increasing Δp and have means ranging from 2/3 to 3/4 of the axial sheet velocity.

The propagation of the mass densities with downstream distance is traced in Fig. 7. With respect to either size (Fig. 7(a)) or velocity (Fig. 7(b)) there is the progression from a dominant second mode, through modes of comparable size, to a dominant first mode as more and more of the mass approaches gas velocity.

A clearer picture of the changes occurring during propagation is given in Fig. 8) by the contour plots of the bivariate size-velocity function. Immediately after formation (Fig. 8)(a)) the large "hill" representing the second, or what may be called the formation mode, is dominant. Only a small peak representing the first, or propagation mode, appears. At the medium downstream distance (Fig. 8 (b)) the propagation peak has sharpened; the formation mode has diminished; and a higher ridge connects the two. Finally the dominant feature of Fig. 8 (c) at the farthest downstream distance is the high propagation mode whose base blends into the extensively altered formation mode.

It is of interest to note that in the studies where bimodal distributions were reported from samples taken at a constant downstream distance [14,15] it was the large size mode which showed the usual changes attributable to variations in injection parameters. This is compatible with the concept that it represented the formation mode while the first mode indicated the stage of propagation. The alternate hypothesis that the two modes resulted from two distinct formation processes is possible, and only velocity data could decide the question.

In the present study the possible existence of bimodal formation processes can be investigated by considering the one-dimensional mass flux distributions. Since vaporization was small, $\underline{f}_F$, the axial flux drop size distribution, should propagate nearly unchanged with z. If definite modes are present at formation they should appear in the flux distribution. Figure 9, which includes both formation and propagation information, indicates that no definite modes are present for Δp = 1.7 atm. The strong bimodal spatial characteristic has almost completely disappeared at downstream locations. It is seen that the flux distribution does remain approximately constant for the three locations with the small shift toward smaller sizes probably being caused by vaporization. Little difference exists between the two curves for higher pressures. The position of the two points at 75 and 100 μm for 2.72 atm could be interpreted as a bimodal formation tendency. However, the data are not extensive enough to warrant a definite conclusion. What is clear is that the two modes considered throughout the discussion of spatial density functions are the result of the drop-gas interactions and are not inherent in the spray formation process.

The formation and propagation results from Figs. 6, 7, and 8 are summarized schematically in Fig. 10 for the situation existing in the present study where the mean velocity at the exit of the atomizer, v_E, is greater than the ambient air velocity, u. Each contour plot of the mass density surface in the size-velocity plane is accompanied by the marginal density functions of D or v alone. The relationship between the spatial and flux drop size distributions is also noted for each case. At the formation and equilibrium conditions the flux and density distributions differ by approximately a constant. Density contours show the progression from a single "hill" formation mode to the bimodal intermediate propagation surface and, finally, the return to a single hill where drops and gas are in velocity equilibrium. The ideal equilibrium condition where the velocity density approaches a delta function was not yet reached at the actual downstream locations sampled (Fig. 8(c)). Reasoning from Fig. 10, the corresponding curves for the case of injection into a higher velocity gas stream can be visualized by inverting the contours and densities with respect to the velocity ordinace. Drops would then accelerate from v_E to u.

CONCLUSIONS

Detailed drop size and velocity measurements made on a spray immediately after formation and during propagation lead to the following conclusions about the role of drop velocity in spray description:

1. Drop velocity in a spray is a statistically distributed variable, the knowledge of which is as important as drop size. Beginning at the shortest downstream distances where a spray may be said to exist, the velocities of drops of a given size are distributed over a range of values usually with a mean substantially different from the mass average injection velocity.

2. Drop concentrations in particular size and velocity ranges as given by the size-velocity density function are strongly dependent on position. This spatial dependence is determined to a large extent by the amount of droplet-gas interaction that has occurred. A wide variation in the shape and modal characteristics of the distribution curves may be found in the same spray simply by sampling at different locations. Unless sampling conditions are very carefully specified, little basis exists for the comparison of different sets of spatial drop size data.

3. Bimodal density functions may be formed by environmental interactions occurring during downstream propagation. In the present case, the selective deceleration of drops according to size produced a transition from a primarily unimodal formation characteristic to a bimodal condition consisting of drops near velocity equilibrium with the gas and those still being decelerated.

4. In many cases, large differences in shape and modal characteristics exist between spatial and flux distributions at the same location. Only in special situations where all drops have closely approached the same velocity are photographic and collection data equivalent.

ORIGINAL PAGE IS
OF POOR QUALITY

REFERENCES

[1] Williams, F. A., "Progress in Spray Combustion Analysis," Proceedings of the Eighth (International) Symposium on Combustion, Williams and Wilkins, Baltimore, 1962, pp. 50-69.

[2] York, J. L., and Stubbs, H. E., "Photographic Analysis of Sprays," Transactions of the American Society of Mechanical Engineers, Vol. 74, No. 7, Oct. 1952, pp. 1157-1162.

[3] Ingebo, R. D., "Vaporization Rates and Drag Coefficients for Isooctane Sprays in Turbulent Air Streams," NACA TN-3265, 1954.

[4] Manning, W. P., and Gauvin, W. H., "Heat and Mass Transfer to Decelerating Finely Atomized Sprays," American Institute of Chemical Engineers Journal, Vol. 6, No. 2, June 1960, pp. 184-190.

[5] Short, W. L., "Some Properties of Sprays Formed by the Disintegration of a Superheated Liquid Jet," Ph.D. Thesis, University of Michigan, 1963.

[6] Groeneweg, J. F., "The Statistical Description of a Spray in Terms of Drop Velocity, Size, and Position," Ph.D. Thesis, University of Wisconsin, 1967.

[7] Benson, G. M., et al., "Fluorescent Technique for Determining The Cross-Sectional Drop Size Distributions of Liquid Sprays," American Rocket Society Journal, Vol. 30, No. 5, May 1960, pp. 447-454.

[8] Rice, E. J., "The Effect of Selected Fluid Parameters on Spatial Drop Size Distribution," Ph.D. Thesis, University of Wisconsin, 1966.

[9] Briffa, F. E. J., and Dombrowski, N., "Entrainment of Air into a Liquid Spray," American Institute of Chemical Engineers Journal, Vol. 21, No. 4, July 1966, pp. 708-717.

[10] Binark, H., and Ranz, W. E., "Induced Air Flows in Fuel Sprays," ASME Paper No. 58-A-284, 1958.

[11] DeCorso, S. M., "Effect of Ambient and Fuel Pressure on Spray Drop Size," ASME Paper No. 59-GTP-3, Mar. 1959.

[12] Heidmann, M. F., "Photography and Analysis of Time Variation in Drop Size Distribution of a Liquid Spray," Proceedings of Fifth International Congress on High Speed Photography, Washington, D.C., Paper No. N-7, Oct. 1960, pp. 519-524.

[13] Marshall, W. R., "Atomization and Spray Drying," Chemical Engineering Progress, Monograph Series, Vol. 50, No. 2, 1954.

[14] Heidmann, M. F., and Foster, H. H., "Effect of Impingement Angle on Drop-Size Distribution and Spray Pattern of Two Impinging Water Jets," NASA TN D-872, 1961.

[15] Bittker, D. A., "Effect of Ambient Air Velocity on Atomization of Two Impinging Water Jets," NASA TN D-2087, 1964.

TABLE I. - SAMPLING SYSTEM SPECIFICATIONS AND OPERATING CONDITIONS

Light sources: Guided air sparks in 0.8 × 19 mm slot
- Maximum energy - 80 joules; 0.1 μf charged to 40 kV
- Flash duration (half peak) - 1.5 to 2.0 μs
- Delay between flashes - continuously variable; nominal values used 9.5 to 74 μs
- Control - spark gap switches pressurized with dry nitrogen

Sampling volume: Thin slab parallel to the spray axis
- Size - 4.0 × 4.0 × 0.2 mm
- Formed by - two 152 mm f/1.2 plano-parabolic, fused-quartz condensing lenses

Fluorescent dye: Uranin (fluorescein)
- Concentration - 5 grams/liter in 95% ethyl alcohol
- Spectral characteristics - absorption peaks at 2500 and 4900 Å; emission peak at 5300 Å.

Camera: Two lens system
- Objective lens - f/3.5, 152 mm operated at f/5.6
- Reimaging lens - f/2.0, 58 mm
- Overall magnification - 25
- Size resolution - 10μ ± 10% (static calibration)
- Working distance - 152 mm
- Depth of field for 10μ objects - ≈220μ

Film: 4 × 5 sheets, ASA 1200
- Development - 12 minutes continuous agitation followed by Monckhoven's intensifier

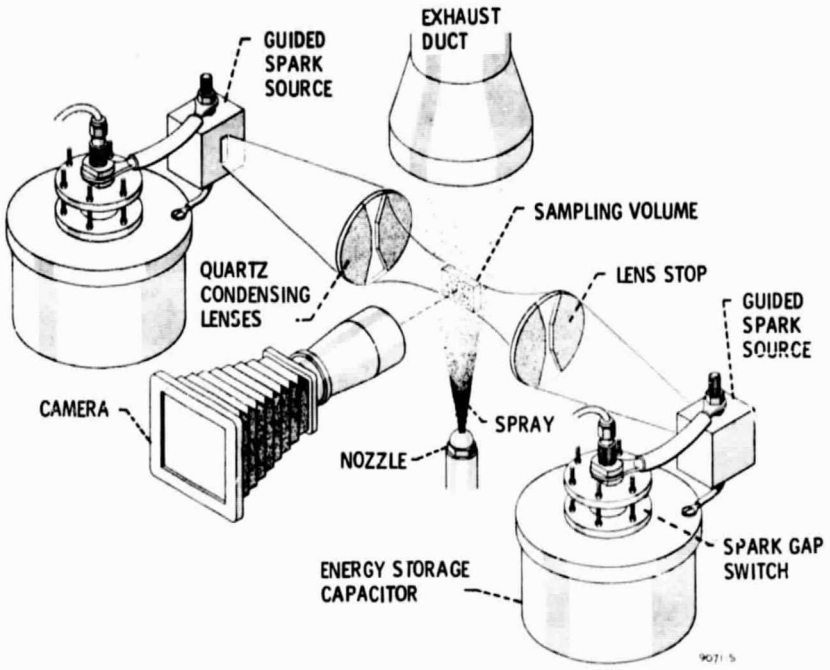

Figure 1. - Experimental arrangement for double-exposure fluorescent photography.

ORIGINAL PAGE IS
OF POOR QUALITY

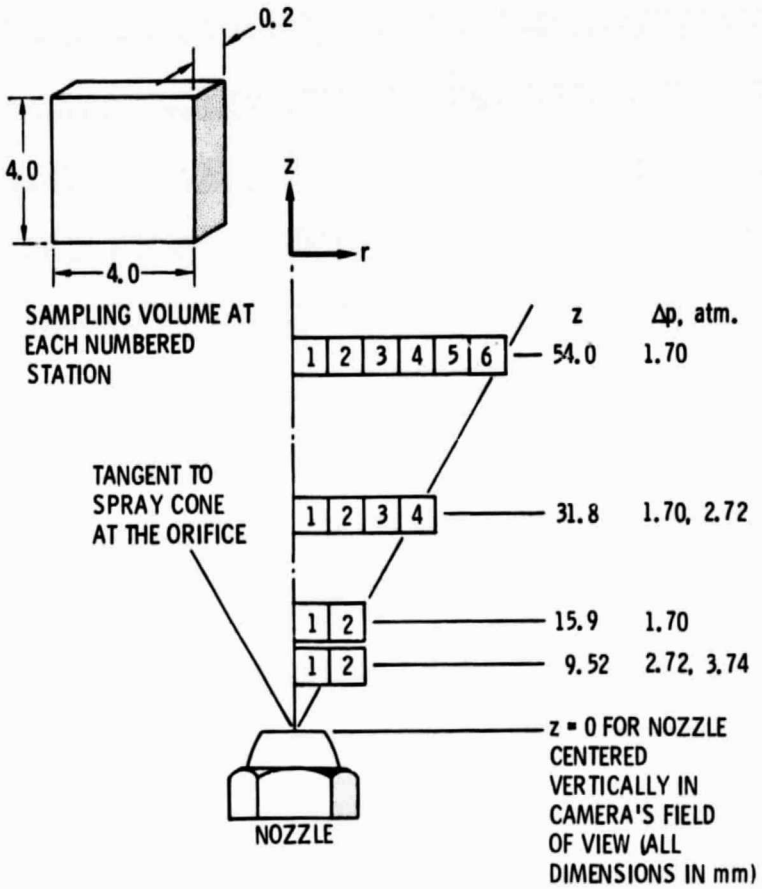

Figure 2. - Sampling geometry and conditions.

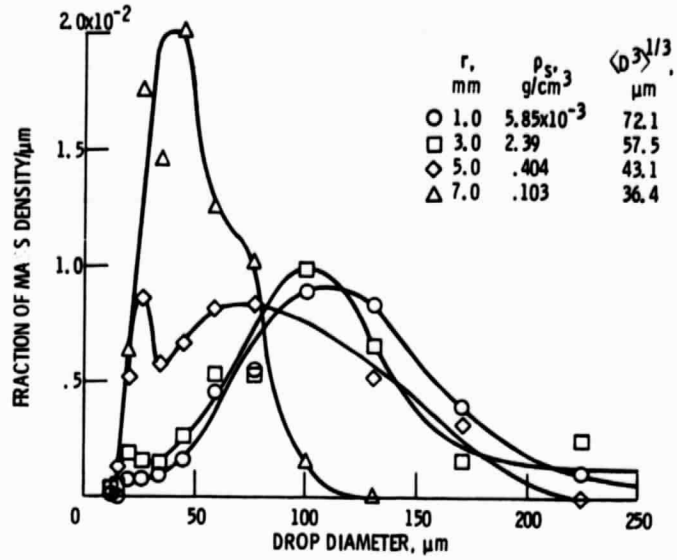

(a) AS A FUNCTION OF DROP SIZE.

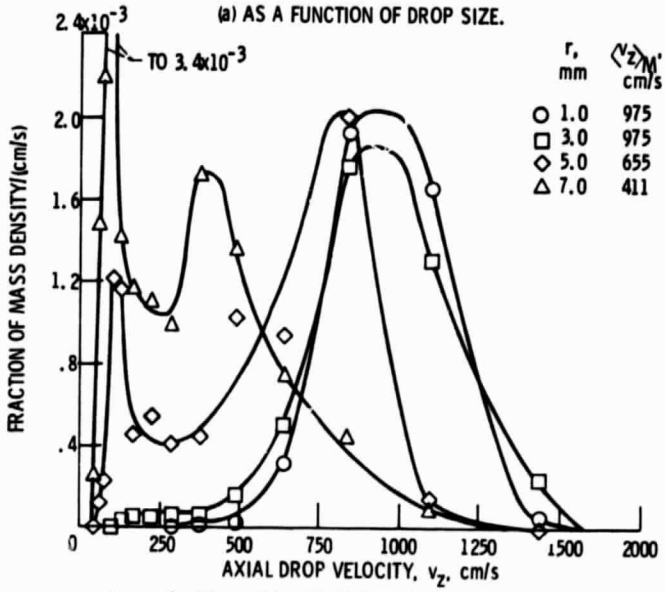

(b) AS A FUNCTION OF AXIAL DROP VELOCITY.

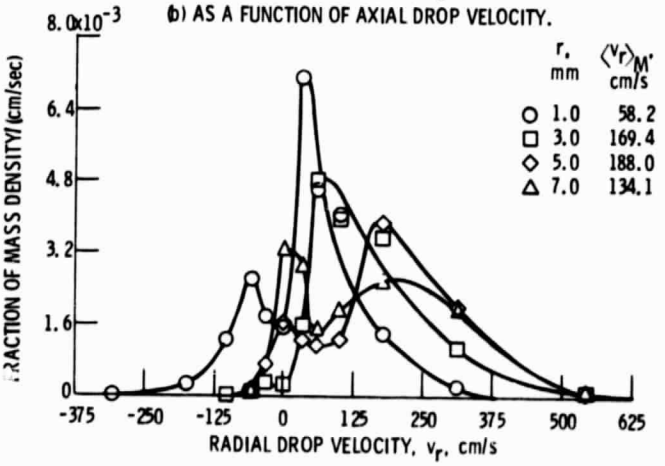

(c) AS A FUNCTION OF RADIAL DROP VELOCITY.

Figure 3. - Mass densities near the surface of formation, Δp = 1.7 atm, z = 15.9 mm.

ORIGINAL PAGE IS
OF POOR QUALITY

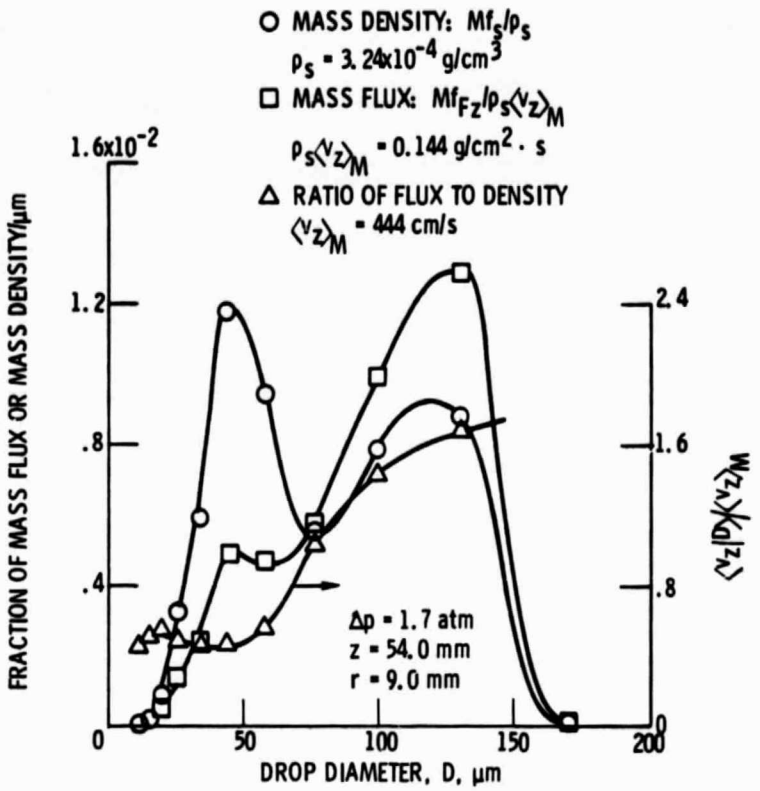

Figure 4. - Comparison of the modal characteristics of spatial and flux distributions at a particular location.

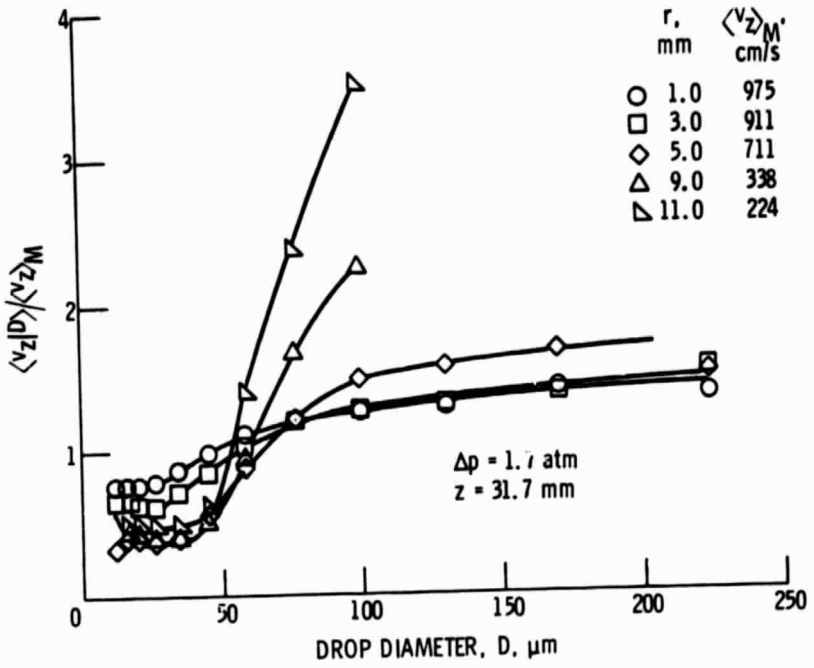

Figure 5. - Expected values of drop velocity as a function of size at several radii at a downstream location.

ORIGINAL PAGE IS
OF POOR QUALITY

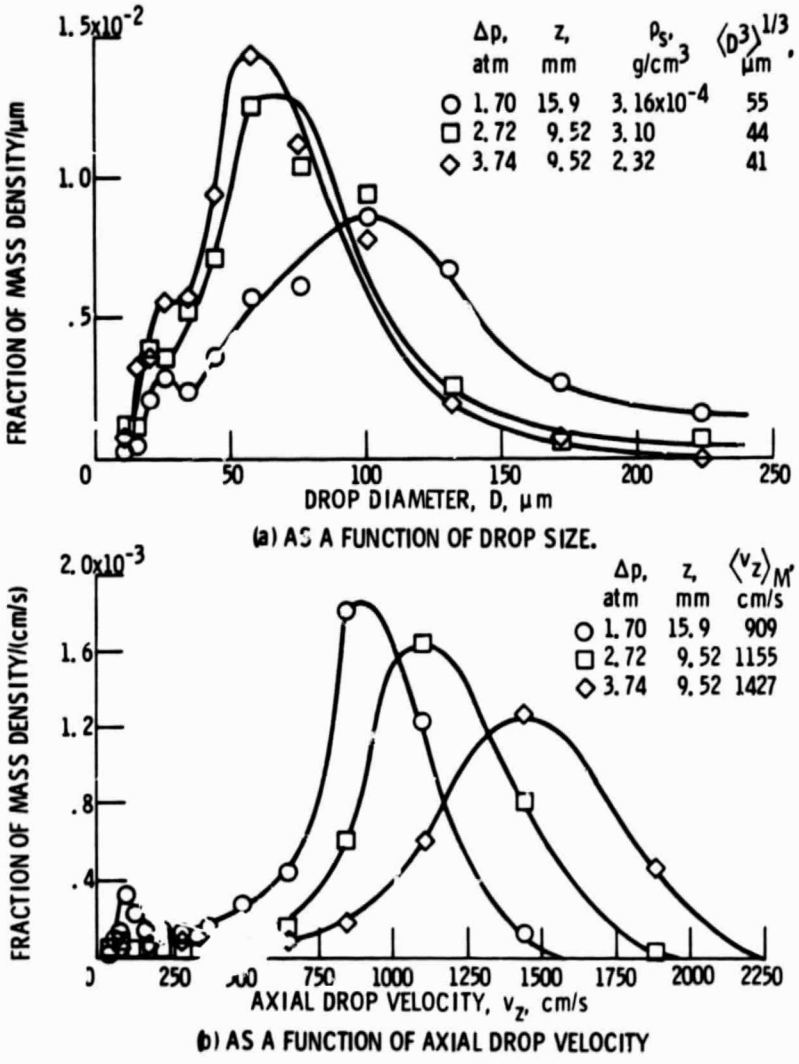

Figure 6. - One-dimensional mass densities near the surface of formation.

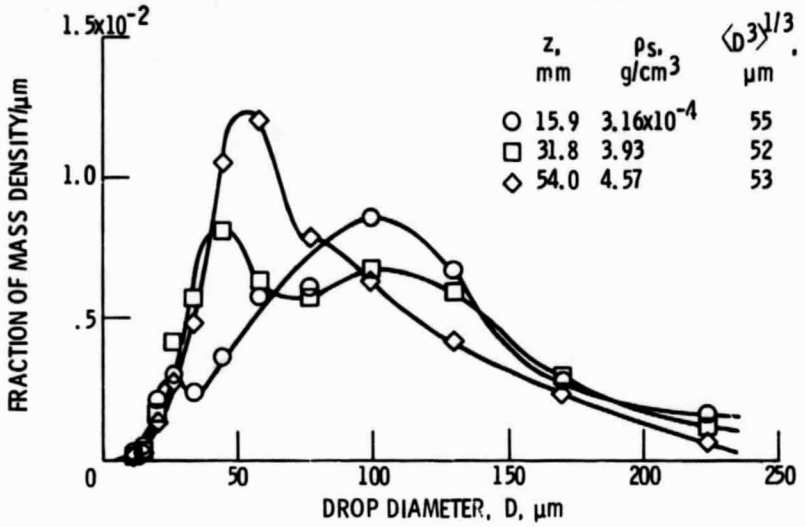

(a) AS A FUNCTION OF DROP SIZE.

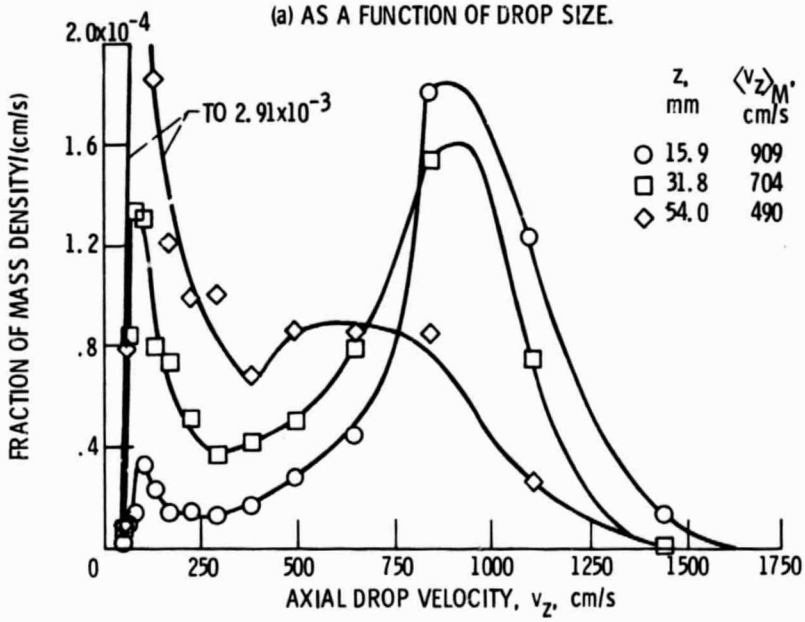

(b) AS A FUNCTION OF AXIAL DROP VELOCITY.

Figure 7. - Propagation characteristics of the one-dimensional mass densities, $\Delta p = 1.70$ atm.

ORIGINAL PAGE IS
OF POOR QUALITY

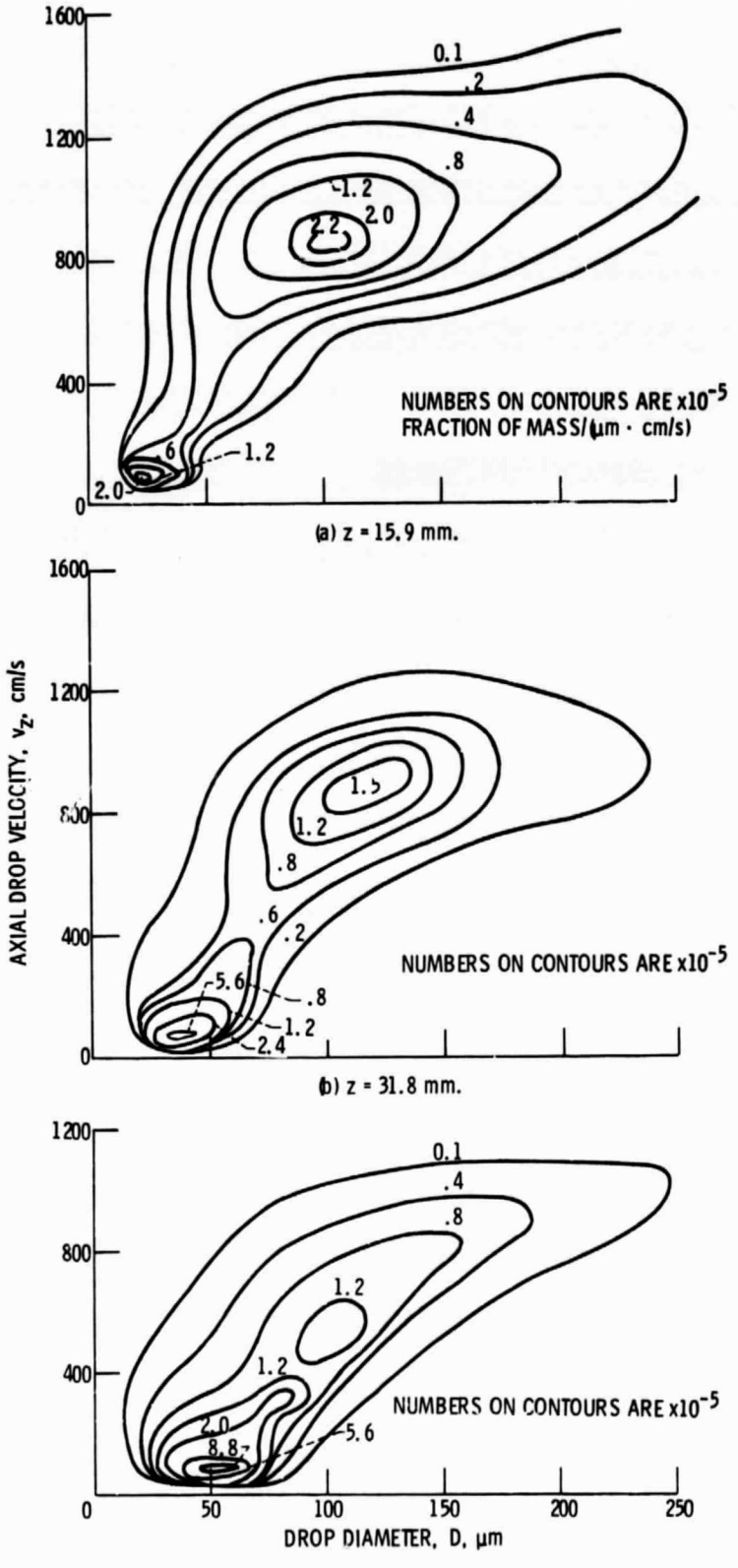

Figure 8. - Contour maps of one-dimensional, bivariate mass densities, $\Delta p = 1.7$ atm.

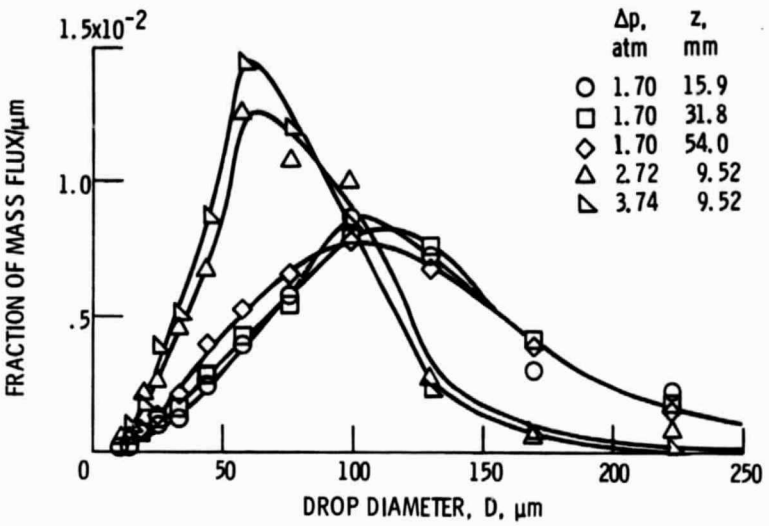

Figure 9. - One-dimensional mass flux distributions.

ORIGINAL PAGE IS
OF POOR QUALITY

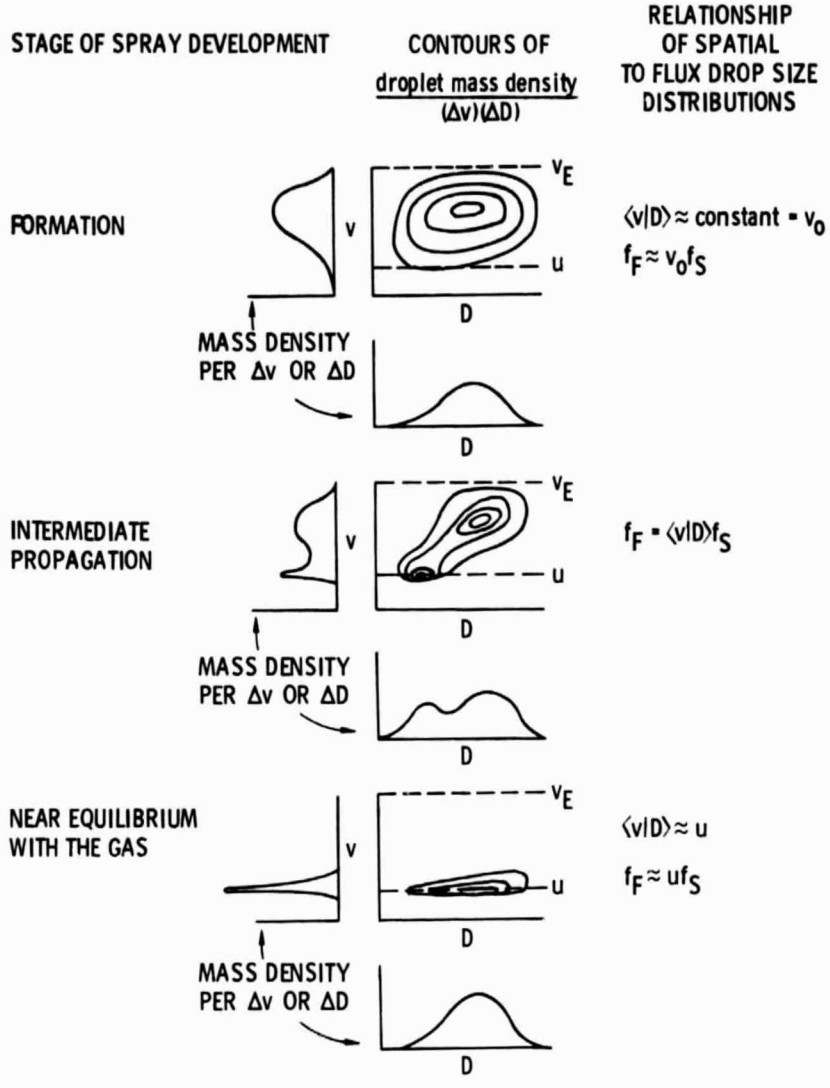

Figure 10. - Schematic formation-propagation characteristics of mass density functions with no vaporization, $v_E > u$.